The Relationship between Binding Models of TMA with Furan and Imidazole and the Molecular Electrostatic Potentials: DFT and MP2 Computational Studies

Tong Liu,[†] Jiande Gu,*,[†] Xiao-Jian Tan,[†] Wei-Liang Zhu,[†,‡] Xiao-Min Luo,[†] Hua-Liang Jiang,*,[†] Ru-Yun Ji,[†] Kai-Xian Chen,[†] Israel Silman,[§,‖] and Joel L. Sussman*,[‖]

Center for Drug Discovery & Design and State Key Laboratory of Drug Research, Shanghai Institute of Materia Medica, Shanghai Institutes for Biological Sciences, Chinese Academy of Sciences, 294 Taiyuan Road, Shanghai 200031, P. R. China, Chemical Process & Biotechnology Department, Singapore Polytechnic, 500 Dover Road, Singapore 139651, Department of Structural Biology, Weizmann Institute of Science, 76100 Rehovot, Israel, and Department of Neurobiology, Weizmann Institute of Science, 76100 Rehovot, Israel

The theoretical investigation of tetramethylammonium (TMA)−imidazole and TMA−furan complexes has been performed to justify the preferred structure of the cation−aromatic complexes predicated by the analysis of molecular electrostatic potential (MEP) maps of isolated aromatic systems. Such maps have been shown to be helpful in predicting the cation binding sites in cation−aromatic complexes. Our computational results show that a large part of the binding energies in the systems studied are contributed by the classical cation−π interaction. However, the optimized structure obtained in the MP2 method might be different from that obtained by the DFT method due to the influence of dispersion forces. Dispersion forces have been found to be important in the systems studied, increasing the binding energies by ∼7% and 20% for the TMA−imidazole and TMA−furan systems, respectively.

Introduction

There is substantial theoretical and experimental evidence for the importance of the cation−π interaction in biological systems.[1−3] This interaction is strong enough to play a significant role in structure and function of biological molecules, including features such as protein folding, local architecture, protein−ligand recognition, and enzymatic activity.[4−9] Recently, Dougherty and co-workers used energy-based criteria to search a protein database composed of 593 proteins. They found that over 25% of all tryptophans in their database experience an energetically significant cation−π interaction.[6] Similarly, Minoux and Chipot[10] analyzed a protein database containing 1718 representative structures for the association of phenylalanine, tyrosine, and tryptophan with arginine and lysine, and they estimated close to 2500 cation−aromatic pairs. In particular, determination of the X-ray structure of *Torpedo californica* acetylcholinesterase (*Tc*AChE, PDB ID code: 1ACE) by Sussman et al.[11] showed that a narrow gorge leading to the active site is lined with 14 conserved aromatic residues which play an important role in facilitating substrate and product traffic to and from the active site and in formation of the enzyme substrate complex. In addition, the cationic side chain of Lys108 is surrounded by the aromatic side chains of Tyr50, Trp52, Try116, and Trp120, forming four cation−π interaction pairs in the X-ray

crystal structure of the protein glucoamylase (PDB ID code: 1GAI), indicating that these cation−π interactions play an important role in stabilizing the local structure around Lys108.[6] Moreover, a series of cation−π interactions between Lys179 and Trp186, Arg211 and Phe225, Arg213 and Phe225, and Lys215 and Tyr 222 have been found in a β sheet of the human growth hormone receptor extracellular domain (PDB ID code: 3HHR), which may contribute to the stability of the β sheet.[4] Therefore, in recent years, there has been increasing interest in this special noncovalent interaction.

The cation−π interaction can be divided into two parts, electrostatic and nonelectrostatic. Theoretical calculations and experiments have demonstrated that the electrostatic term is the major component.[3,4,12,13] Dougherty and co-workers[4,5,14] demonstrated that analysis of the molecular electrostatic potential (MEP) maps of isolated aromatic rings can usually provide a reliable assignment of the cation-binding site. Thus. the MEP of benzene allows one to conclude that the cation binding site is over the plane of the benzene ring.[14] This prediction is in good agreement with quantum chemical assignments.[8,15−17] Since the MEP can be derived directly from the wave function[18] and can be calculated relatively rapidly, it is much used in theoretical chemical calculations.[19,20] Thus, MEP analysis in the study of cation−π interactions will indeed provide a valuable tool.

However, a problem arose when MEP analysis was used to predict the potential cation binding sites for furan and imidazole. The three-dimensional MEP maps of these two aromatics are similar.[14] In both, there is no obvious negative area above the aromatic ring. The most negative part of the electrostatic potential for furan is outside the aromatic ring adjacent to the oxygen atom. The presence of nitrogen atoms of imidazole system attracts the most parts of the negative electrostatic potential around the imino moiety. Thus, the MEP maps suggest

* Corresponding authors. Please address correspondence and requests for reprints to: Prof. Hua-Liang Jiang, Shanghai Institute of Materia Medica, Chinese Academy of Sciences, 294 Taiyuan Road, Shanghai 200031, P. R. China. Phone: +86-21-64311833, ext. 222. Fax: +86-21-64370269. E-mail: hljiang@mail.shcnc.ac.cn or jiang@iris3.simm.ac.cn.
† Shanghai Institutes for Biological Sciences, Chinese Academy of Sciences.
‡ Chemical Process & Biotechnology Department, Singapore Polytechnic.
§ Department of Structural Biology, Weizmann Institute of Science.
‖ Department of Neurobiology, Weizmann Institute of Science.

that it is unlikely that a cation can be stabilized above either of these two aromatic rings to form a stable complex. Computational results on several cation–imidazole systems support this predication[8,14,21] and indicate that only "end-on" nitrogen complexes represent a true minimum in the systems. However, our recent theoretical study of the NH_4^+–furan system[8] suggests that the center of positive charge of NH_4^+ lies over the aromatic ring, forming a typical cation–π complex. Predicating cation-binding sites on aromatics by only considering the MEP maps of isolated aromatics seems unconvincing. Our earlier studies of the TMA–pyrrole system showed that dispersion interactions must be taken into account and contribute about 25% of the total binding energy.[22] Due to the influence of dispersion interactions, the positive center of TMA moves away from the most negative area in the MEP map of pyrrole. Like pyrrole, both furan and imidazole contain heteroatoms in their aromatic rings. For cation–furan and cation–imidazole complexes such as NH_4^+–furan (imidazole) and TMA–furan (imidazole), the presence of the dispersion interaction might be strong enough to change the stable geometry predicted according to the MEP analysis.

In the following, a theoretical investigation of the MEP maps of furan and imidazole is performed in order to reveal the nature of different cation binding sites in these two rings. On the basis of calculations using density function theory (DFT) and Möller–Plesset second-order perturbation (MP2) approaches, the influence of dispersion interactions in TMA–furan and TMA–imidazole systems are also assigned.

Calculation Methods

Our previous investigation showed that the B3LYP exchange-corrlation functional of density-functional theory method could provide geometric and thermodynamic parameters in comparison with the Möller–Plesset second-order perturbation (MP2) and experimental results for some cation–π systems;[9,16,23–25] thus, local minima of the TMA–furan and TMA–imidazole complexes were fully optimized using the B3LYP method. Wesolowski et al. pointed out that PW91 exchange functional appears as the most reliable for calculating the weak van der Waals complexes between benzene and X (X = O_2, N_2, CO).[26,27] Perdew et al.[28] stated that PW exchange functional is best used in conjunction with the corresponding correlation (the PWPW functional), since in this case the errors in exchange and correlation contributions tend to cancel out. Therefore, the geometries of the two complexes were also optimized using the PW91PW91 functional. To investigate the effect of dispersion interaction, the geometries of these two complexes were further optimized with the MP2 approach.[29–32] The 6-31G** and 6-31+G** basis sets were employed in the all procedures for ensuring a correct description of the complexes. Vibrational frequency calculations were then carried out for each optimized structure to verify the reasonability of the optimized structure. The geometries of TMA, furan, and imidazole were also optimized using the three theoretical methods with the two basis sets, and thus, binding energies between TMA and the aromatics were calculated using the energy parameters. The calculated binding energies were corrected by the basis set superposition error (BSSE) using the counterpoise method of Boys and Bernardi.[33]

All quantum chemistry calculations were carried out with Gaussian 98 software[34] on a Power Challenger R-10000 supercomputer.
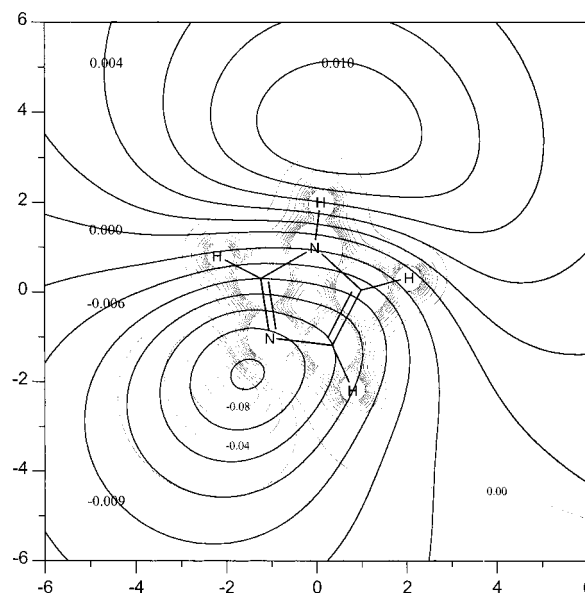

Figure 1. Electrostatic potential map of imidazole in the B3LYP/6-31+G** method. The thin line represents the map on imidazole plane. The contour spacing is 0.1 au for the positive part and 0.02 au for the negative part. The thick line represents the ESP 3.0 Å above the imidazole. The contour spacing is 0.002 au for the positive part and 0.003 au for the negative part. The unit of axes is in Å.

Results and Discussions

Molecular Electrostatic Potential Analysis. The molecular electrostatic potentials (MEPs) of furan and imidazole were calculated at the B3LYP/6-31+G** level based on their optimized geometries. The sliced two-dimensional contour maps of the MEPs of the two aromatics are depicted in Figures 1 and 2. By showing the values in a manifold of spatial locations around the molecule, such a representation provides more detailed information concerning electrostatic potential distribution.

The MEP map in the imidazole plane shows clearly that the most negative part of the electrostatic potential of this molecule is outside the ring, ~1.5 Å from the imino nitrogen atom. Taking into account van der Waals radii, this location is in good agreement with the location of the cation, 2.7 Å away from the imino nitrogen atom in the end-on NH_4^+–imidazole complex.[8]

Away from the imidazole plane, the slices show that the negative center does not move much and no other negative minimum is observed. The slice 3 Å above the molecular plane of imidazole in Figure 1 clearly shows that the negative electrostatic potential center still lies outside the five-membered ring. One can thus conclude that there is no location for formation of a normal cation–π complex above the ring. This is in agreement with previous theoretical studies on various cation–imidazole systems.[8,14,21]

The MEP map for furan in the plane of the ring has similar characteristics. The most negative area of electrostatic potential in this plane lies outside the ring, ~1.5 Å away from the oxygen atom. In the optimized NH_4^+–furan complexes as for the corresponding imidazole complex, the distance of 2.7 Å between the oxygen atom of furan and the N atom of NH_4^+ is in keeping with the known van der Waals radii. Although the detailed electrostatic potential distributions in the planes of the furan and imidazole rings are different, the distances between the negative minima and the corresponding heteroatoms, the oxygen atom of furan and the imino nitrogen atom of imidazole, are about 1.5 Å, which leads to similar distances between the
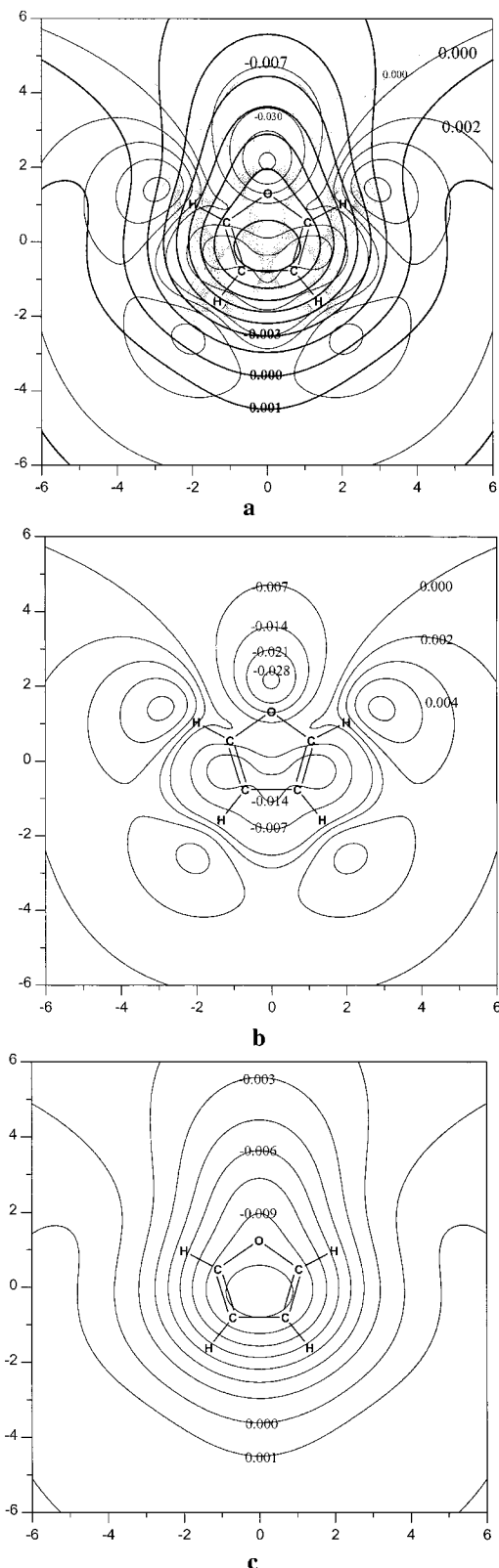
Binding Models of TMA with Furan and Imidazole

J. Phys. Chem. A, Vol. 106, No. 1, 2002 **159**

Figure 2. Electrostatic potential map of furan at the B3LYP/6-31+G** level. (a) The light thin line represents the map in furan plane. The contour spacing is 0.1 au for the positive parts and 0.01 au for the negative parts. The thin line represents the map 1.5 Å above the furan plane. The contour spacing is 0.002 au for the positive parts and 0.007 au for the negative parts. The thick line is the ESP map 3.0 Å above the furan plane. The contour spacings are 0.0015 and 0.001 au for the positive and negative parts, respectively. The unit of the axes is in the angstroms. (b) The sliced electrostatic potential maps 1.5 Å above furan plane. For details, see panel a. (c) The sliced electrostatic potential map 3.0 Å above furan plane. For details, see panel a.

positive center of cation and the heteroatom. The results suggest that the location of negative minimum is of importance to cation binding site.

The sliced MEP maps above the plane of the furan ring show that the location of the negative minimum changes dramatically. It moves toward oxygen atom in the plane 0.75 Å above furan. The slice 1.5 Å above aromatic plane shows that this most negative area directs toward to the oxygen atom further. At the same time, a second negative electrostatic potential area appears. As the slice moves away from the plane of the ring, this second negative electrostatic potential strengthens, and the center of it shifts to the centroid of furan, while the negative electrostatic potential adjacent the oxygen atom moves inward. Finally, these two negative areas merge. Thus, the MEP map 3.0 Å above the plane of the ring displays only one negative electrostatic potential area, and the negative minimum is located above the five-membered ring of furan. If this prediction is correct, it would be expected that a cation$-\pi$ complex would form in which the cation would align with this electrostatic potential minimum above the ring. Quantum chemistry studies on the NH_4^+-furan system are in agreement with this assignment. NH_4^+ binds to the π system of furan to form a perfect cation$-\pi$ complex.[8] The distance between the N of the onium and the plane of the furan ring is ~2.3 Å.

The sliced two-dimensional contour maps of the MEPs of imidazole and furan show that electrostatic potential distributions in the two aromatic systems are different. Only one potential cation binding site is predicted in the cation$-$imidazole complex (end-on nitrogen binding), while two possible cation binding sites are predicted for the cation$-$furan complex (end-on oxygen binding and cation$-\pi$ binding). These predications are in good agreement with other computational studies.[13,21]

Molecular Structure. To verify the predicted cation binding sites for imidazole and furan obtained by MEP analysis, the structures of the TMA$-$furan and TMA$-$imidazole complexes were optimized at both the DFT (B3LYP and PW91PW91) and the MP2 theoretical levels.

TMA$-$Imidazole Complex. As expected from the MEP analysis of imidazole, all the starting structures of TMA$-$imidazole complex (Figure 3a) converged into one geometry at the B3LYP/6-31G** level. The vibrational analysis result for all positive frequencies at this level confirms that this structure is the local minimum on the potential energy surface. The optimized structure is depicted in Figure 4a along with the important geometric parameters. The cation rests in the plane of the imidazole at the position corresponding to the negative minimum predicted by MEP analysis. The direct interactions between the cation and the aromatic ring involve three hydrogen atoms of TMA (one from each methyl group) and the imino nitrogen atom (N_3) of imidazole (r_1 to r_3 in Figure 4a). For the B3LYP results, the $N_3 \cdots H$ distance varies from 2.410 to 2.617 Å. Adding diffuse functions in the basis sets leads to only slight increases in $N_3 \cdots H$ distances (about 0.03 Å for r_1 and r_3 and 0.07 Å for r_2). The distances between the N atom of TMA and the imino nitrogen atom of imidazole are 3.677 Å with the basis set of 6-31G** and 3.726 Å of 6-31+G**. Assuming an additional 1.0 Å of the C$-$H bond length, those distances consistent with the value of 2.7 Å for the NH_4^+-imidazole complex.

The optimized structure predicated by the PW91PW91 level of calculation is basically the same as that by the B3LYP. The distances between N atom of TMA and imino nitrogen of imidazole vary from 3.618 Å (6-31G**) to 3.663 Å (6-31+G**), about 0.06 Å shorter than the B3LYP predication.
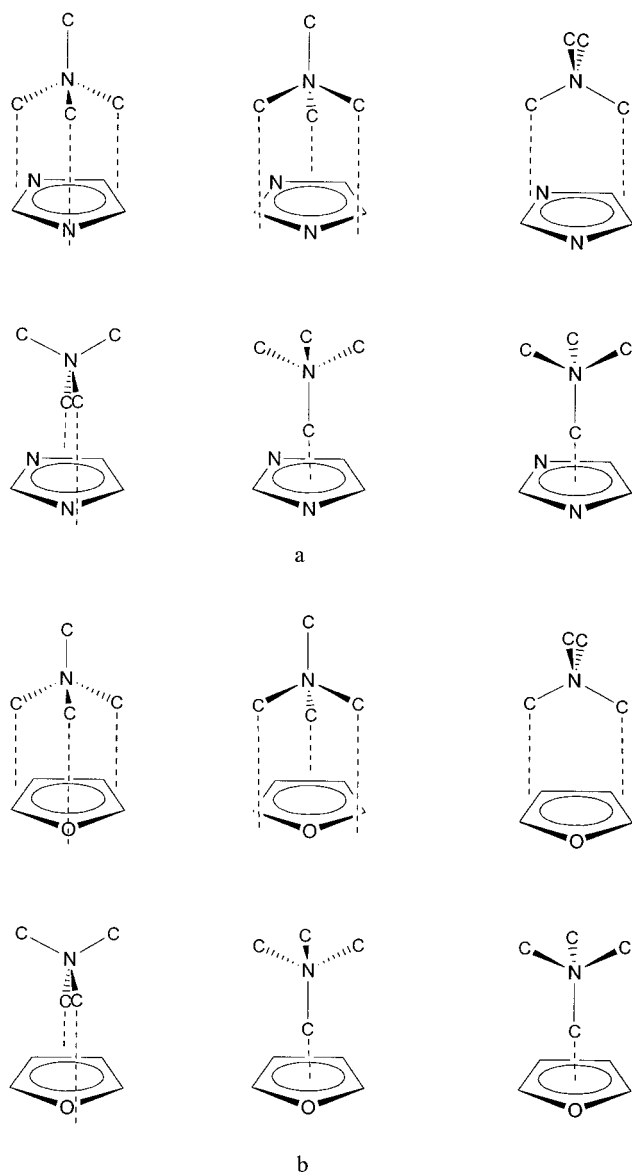
160 *J. Phys. Chem. A, Vol. 106, No. 1, 2002*

Liu et al.

Figure 3. Initial structures of the TMA−furan (a) and TMA−imidazole (b) complexes. Hydrogen atoms are omitted for clarity.

It is obvious that the $N_3 \cdots H$ distances are sensitive to the theoretical methods used in the calculations. The MP2 method predicts values of intermolecular distances about 0.1−0.2 Å shorter than those from the B3LYP method. Since it is well-known that the B3LYP method does not involve dispersion interactions, one can attribute the predicated difference between MP2 method and B3LYP method to dispersion interactions being taken into account in the MP2 method.[35−37] The interaction between TMA and imidazole is intensified by the dispersion interactions between the $N_3 \cdots H$ pairs. Compared with the results at the PW91PW91 level, the intermolecular distance calculated at the MP2 level is only 0.03 Å shorter. The similarity of predicted structures between the MP2 approach and the PW91PW91 approach is in agreement with the results of Wesolowski.[26,27]

It is noteworthy that the $N_3 \cdots H$ distances of ∼2.3−2.6 Å and the C−H$\cdots N_3$ angles of ∼150° are in the ranges of values of typical hydrogen bonds proposed by Scheiner[38] and Jeffery.[39] This suggests that the TMA−imidazole complex is further strengthened by the three pairs of C−H$\cdots N_3$ hydrogen bonding interactions.

TMA−Furan Complex. Six possible structures of TMA−furan were chosen as the initial geometries (Figure 3b) to find out the real minima of the complex. As suggested by the analysis of the MEP of furan, the starting structures converged into two different structures at the B3LYP level using both 6-31G** and 6-31+G** basis sets. These two local minima correspond to the two negative minima in the MEP map of furan. Vibrational analysis shows that both structures are true local minima on the potential energy surface. Panels b and c of Figure 4 show the optimized structures and the important geometric parameters. The first optimized structure is similar to that of the TMA−imidazole complex, with the nitrogen atom of the cation lying in the plane of the furan ring. The distance between the nitrogen atom of TMA and the oxygen atom of furan is calculated to be 3.817 Å at the B3LYP/6-31+G** level, which is similar to the distance between the N atom of TMA and the N_3 of imidazole at the same level. This location is not unexpected if one bears in mind the similarity between the MEP maps of imidazole and furan in the plane of the aromatic rings. Thus, for a given cation, similar locations of the minima on the MEP maps seem to produce similar cation binding sites in the cation−aromatic systems. The calculated $O_1 \cdots H$ distances of ∼2.5 Å and C−H$\cdots O_1$ angles of ∼150° predicted at the B3LYP level are characteristic of C−H$\cdots O$ hydrogen bonds. Similar to the TMA−imidazole complex, this TMA−furan conformer displays three C−H$\cdots O_1$ hydrogen bonding interactions.

In the second local minimum structure optimized at the B3LYP level, the cation assumes a position above the plane of furan (Figure 4c), which corresponds to the minimum MEP above plane predicted for furan. Vertical projection shows that the positive center of the cation coincides with the most negative area of electrostatic potential in the slice 3 Å above the plane of the furan ring. This conformer has typical cation−π characteristics. The distance between the N atom of TMA and the plane of the furan ring is predicted to be 4.16 Å at the B3LYP/6-31G** level, consistent with the B3LYP prediction for the NH_4^+−furan complex of about 3.0 Å.[8] Thus, both the cation binding sites predicted by MEP analysis are indeed found by the B3LYP procedure.

For the TMA−imidazole complex, both the B3LYP and PW91PW91 methods give similar local minimum structures, whereas optimizations for the TMA−furan complex using the PW91PW91 method at both the 6-31G** and 6-31+G** levels of theory do not converge to the end-on cation−furan structure and only the cation−π structure is obtained (Figure 4c). It is noteworthy that the optimization was also performed with the PW91PW91 method using the end-on TMA−furan structure obtained at the B3LYP level as the start point. The structure converges to the classical cation−π structure finally. The result indicates that the different exchange-correlation functionals significantly affect the potential energy surface of TMA−furan system. The distances between N of TMA and furan plane are 4.12 Å with the 6-31G** basis set and 4.16 Å with the 6-31+G**, ∼0.05 Å shorter than those from the B3LYP predication.

Both optimized B3LYP structures were reoptimized with the MP2 method with the basis set of 6-31G**. Similar to the result at the PW91PW91 method, only the classical cation−π structure is obtained. The calculated distance between the N atom of TMA and the plane of the furan ring is 4.09 Å, about 0.07 and 0.02 Å shorter than those using the B3LYP and PW91PW91 method, respectively. This difference may be due to the different amount of electron correlation taken into account in the different method, which will be discussed later. To check the influence of diffuse
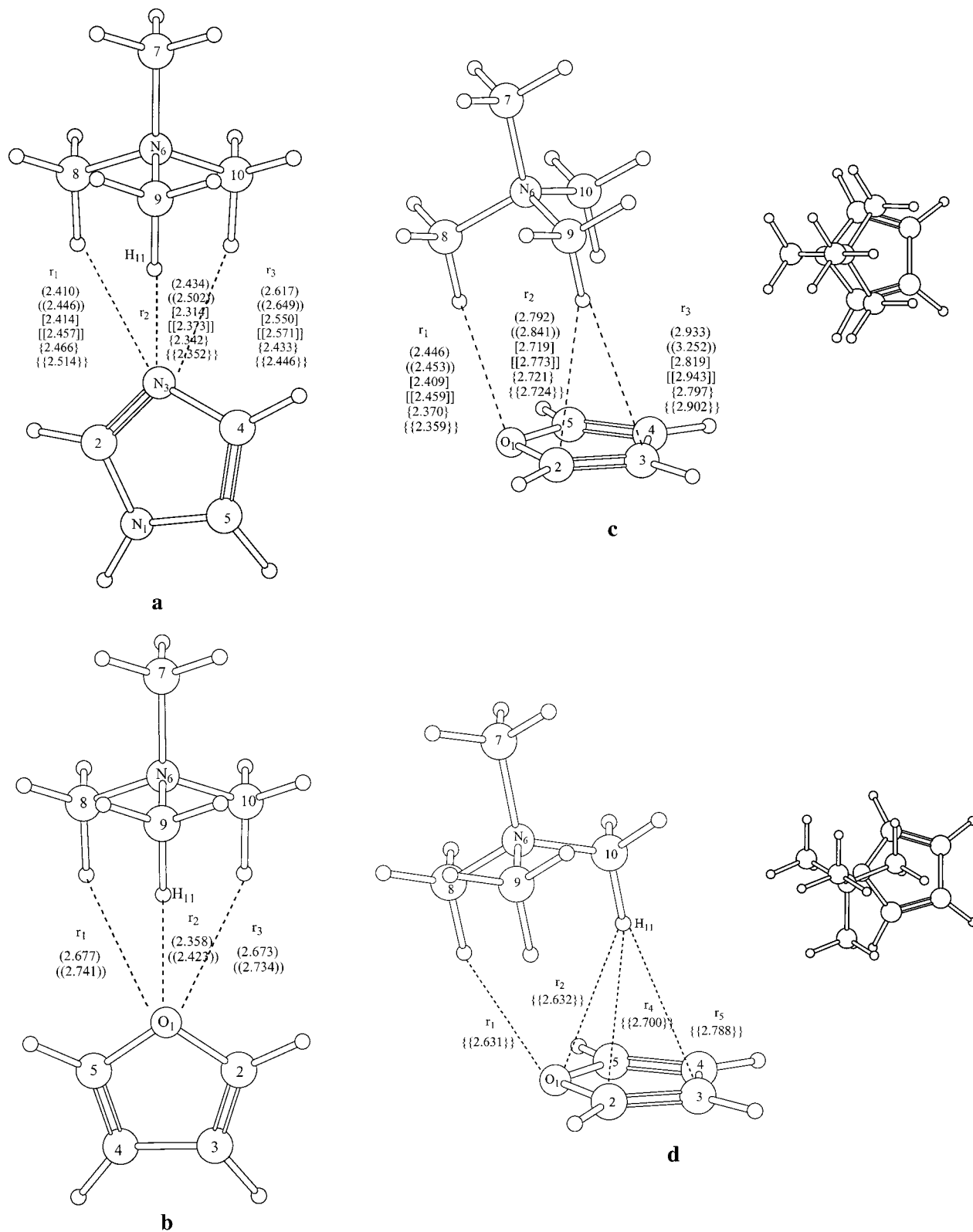
Figure 4. Optimized structures and important geometric parameters of the TMA−imidazole (a) and of the plane structure (b), the typical cation−π form (c), and the distorted cation−π form (d) of TMA−furan complex obtained by the B3LYP and the MP2 methods. Bond lengths and distances are in Å. Data in parentheses and double parentheses are produced by the B3LYP/6-31G** and the B3LYP/6-31+G** methods, respectively; data in brackets and double brackets are calculated with the PW91PW91/6-31G** and the PW91PW91/6-31+G** methods, respectively; data in curly brackets and double curly brackets are the MP2/6-31G** and the MP2/6-31+G** results, respectively. The vertical projections of typical cation−π and distorted cation−π forms of TMA−furan complex are also depicted for clarity.

function, the stable structures were further optimized at the MP2/6-31+G** level. Two optimized structures were thus obtained. One is basically the same as the local minimum obtained at the MP2/6-31G** level. Due to the introduction of the diffuse

function, a small increase of 0.02 Å can be observed for the distance between N of TMA and the plane of the furan ring. In the second optimized structure (Figure 4d), although the TMA is located above the plane of furan ring, the vertical projection

TABLE 1: Energy Properties of TMA−Furan and TMA−Imidazole Complexes Evaluated at the DFT and the MP2 Methods

TMA−Imidazole Complex

	E (au)			ΔE (kcal mol^{-1})	BSSE (kcal mol^{-1})		ΔE^{BSSE} (kcal mol^{-1})
	TMA	imidazole	complex		TMA	imidazole	
B3LYP/6-31G**	−214.1812869	−226.2230930	−440.4317289	−17.16	0.0629	1.9914	−15.11
B3LYP/6-31+G**	−214.1830148	−226.2353836	−440.4416391	−14.58	0.1087	0.2253	−14.25
PW91PW91/6-31G**	−214.0664760	−226.1421637	−440.2388678	−18.97	0.0351	1.9868	−16.95
PW91PW91/6-31+G**	−214.0689925	−226.1549890	−440.2497479	−16.17	0.1139	0.2385	−15.82
MP2/6-31G**	−213.4685511	−225.5525174	−439.0528474	−19.94	0.3466	2.7146	−16.88
MP2/6-31+G**	−213.4733291	−225.5684632	−439.0713121	−18.52	0.8412	1.3043	−16.37

TMA−Furan Complex

		E (au)			ΔE (kcal mol^{-1})	BSSE (kcal mol^{-1})		ΔE^{BSSE} (kcal mol^{-1})
		TMA	furan	complex		TMA	furan	
plane form	B3LYP/6-31G**	−214.1812869	−230.02737130	−444.2197151	−6.94	0.1882	1.6084	−5.14
	B3LYP/6-31+G**	−214.1830148	−230.03820930	−444.2294294	−5.15	0.1025	0.2256	−4.82
typical cation−π	B3LYP/6-31G**			−444.2203510	−7.34	0.1963	1.4939	−5.65
	B3LYP/6-31+G**			−444.2296454	−5.28	0.1083	0.2789	−4.89
	PW91PW91/6-31G**	−214.0664760	−229.9425052	−444.0234745	−9.09	0.1992	1.5564	−7.33
	PW91PW91/6-31+G**	−214.0689925	−229.9538010	−444.0337370	−6.87	0.1100	0.3243	−6.44
	MP2/6-31G**	−213.4685511	−229.3421658	−442.8268356	−10.11	0.6308	2.2724	−7.21
	MP2/6-31+G**	−213.4733291	−229.3564464	−442.8448145	−9.44	0.9390	1.5215	−6.98
distorted cation−π	MP2/6-31+G**			−442.8452486	−9.71	1.0007	1.7261	−6.98

shows that the N atom of TMA is outside the ring. The optimized structure is thus a distorted cation−π structure. Vibrational analysis confirms that this structure represents a true local minimum. The distance between the N atom of TMA and the plane of the furan ring is 3.81 Å, ∼0.26 Å shorter than the corresponding distance in the more characteristic cation−π structure.

According to the MEP analysis for furan, the cation is expected to bind both in the plane of the ring and above it. However, the MP2 calculations at both 6-31G** and 6-31+G** levels show that the cation cannot rest in the plane of the furan ring. The main reason might be the dispersion interaction, which can be given in the MP2 method.[35−37] Above the plane of the furan ring, it is easier for dispersion interactions to occur between the H atoms of TMA and the heavy atoms of furan. With regard to the distorted cation−π form obtained at the MP2/6-31+G** level, it is clear from the vertical view of the structure that the positive charge center of the cation does not coincide with the negative minimum of the MEP map in the plane 3 Å above the furan ring. This will weaken the electrostatic interaction, but this energy loss may be compensated by better dispersion interactions. H_{11} lies above the center of furan, forming six dispersion interaction pairs. It should be noted that the MP2/6-31G** method cannot trap this distorted cation−π form either, even if optimization is initiated from the structure produced by MP2/6-31+G**. The results obtained indicate that diffuse functions enhance the dispersion interaction in such systems.

Energetic Properties. *TMA−Imidazole Complex.* The calculated binding energies of the TMA−imidazole system are summarized in Table 1. The BSSE corrected binding energy of the system is −15.11 kcal mol^{-1} at the B3LYP/6-31G** level and −14.25 kcal mol^{-1} at the B3LYP/6-31+G** level. The total BSSE is as low as 0.33 kcal mol^{-1} at the B3LYP/6-31+G** level, suggesting that the basis set is adequate. On the other hand, the binding energies of TMA−imidazole determined by the PW91PW91 method with the 6-31G** and 6-31+G** basis sets are, after the BSSE correction, −16.95 and −15.82 kcal mol^{-1}, respectively. Those predicated results are more than 1.5 kcal mol^{-1} stronger than the values at the B3LYP level. At the MP2 level, the BSSE corrected binding energies are −16.88

kcal mol^{-1} for 6-31G** and −16.37 kcal mol^{-1} for 6-31+G**. The similarity of binding energy between the MP2 method and the PW91PW91 method is consistent with the conclusion of Wesolowski.[26,27] Also, the calculated binding energy in this study is very close to Pullman's theoretical result at the MP2/6-31G^{aa} level (−16.27 kcal mol^{-1}).[21] The total BSSE of ∼2.1 kcal mol^{-1} at the MP2 level seems too large. However, our previous study on the TMA−benzene system showed that the predicted binding energy at the MP2/6-31+G** level provides a result very close to the experimental value and that using more sophisticated basis sets does not produce a substantial change.[22]

TMA−Furan Complex. The energy properties of the TMA−furan complex are also listed in Table 1. For the B3LYP method with the basis sets of 6-31G**, the BSSE corrected binding energy is −5.14 kcal mol^{-1} for the end-on structure and −5.65 kcal mol^{-1} for the typical cation−π structure. After adding the diffuse function into the basis sets, the calculated energies are −4.82 kcal mol^{-1} for the end-on form and −4.89 kcal mol^{-1} for the cation−π form, a difference of 0.07 kcal mol^{-1}. Thus, there is no significant difference in binding energy between the two local minima. Our earlier study on the NH_4^+−furan system at the B3LYP/6-31G** level shows that the plane structure is 1.5 kcal mol^{-1} more stable than the cation−π complex.[8] Since in the end-on structure of NH_4^+−furan one N−H bond points toward the oxygen atom of furan and thus forms a strong classical hydrogen bond, this result is possible. The BSSE corrected binding energy for the end-on structure of the TMA−furan complex is about 10 kcal mol^{-1} weaker than that for TMA−imidazole complex.

For the only structure (cation−π form) obtained by the PW91PW91 method, the BSSE corrected binding energies are −7.33 kcal mol^{-1} for the PW91PW91/6-31G** level and −6.44 kcal mol^{-1} for the PW91PW91/6-31+G** level. The binding energies predicated by the PW91PW91 method are about 1.7 kcal mol^{-1} more stable than those by the B3LYP method, which is in agreement with the small intermolecular distance obtained at the PW91PW91 level (Figure 4).

As expected, the binding energy calculated at the MP2 level is stronger than that obtained by the DFT method. After the BSSE correction, the binding energy of the typical cation−π form is −7.21 kcal mol^{-1} at the MP2/6-31G** level and −6.98

Binding Models of TMA with Furan and Imidazole

J. Phys. Chem. A, Vol. 106, No. 1, 2002 **163**

TABLE 2: Energy Properties of TMA−Furan and TMA−Imidazole Complexes Evaluated at the HF, DFT, and MP2 Methods on the Geometries Obtained by MP2/6-31+G Optimization**

TMA−Imidazole Complex

	E (au)			ΔE (kcal mol⁻¹)	BSSE (kcal mol⁻¹)		ΔE^BSSE (kcal mol⁻¹)
	TMA	imidazole	complex		TMA	imidazole	
MP2/6-31+G**	−213.4733291	−225.5684632	−439.0713121	−18.52	0.8412	1.3043	−16.37
HF/6-31+G**//MP2/6-31+G**	−212.7040198	−224.8295288	−437.5547389	−13.30	0.1445	0.3702	−12.79
B3LYP/6-31+G**//MP2/6-31+G**	−214.1808543	−226.2352176	−440.4409705	−15.62	0.1049	0.2481	−15.27
PW91PW91/6-31+G**//MP2/6-31+G**	−214.0662203	−226.1546598	−440.2483157	−17.22	0.1017	0.2622	−16.86

TMA−Furan Complex

		E (au)			ΔE (kcal mol⁻¹)	BSSE (kcal mol⁻¹)		ΔE^BSSE (kcal mol⁻¹)
		TMA	furan	complex		TMA	furan	
cation−π	MP2/6-31+G**	−213.4733291	−229.3564464	−442.8448145	−9.44	0.9390	1.5215	−6.98
	HF/6-31+G**//MP2/6-31+G**	−212.7040198	−228.6375992	−441.3473743	−3.61	0.1657	0.3532	−3.09
	B3LYP/6-31+G**//MP2/6-31+G**	−214.1808543	−230.0380739	−444.2286656	−6.11	0.1306	0.2946	−5.68
	PW91PW91/6-31+G**//MP2/6-31+G**	−214.0662203	−229.9534850	−444.0322030	−7.84	0.1247	0.3283	−7.39
distorted cation−π	MP2/6-31+G**			−442.8452486	−9.71	1.0007	1.7261	−6.98
	HF/6−3+G**//MP2/6-31+G**			−441.3471854	−3.49	0.1814	0.3940	−2.91
	B3LYP/6−3+G**//MP2/6-31+G**			−444.2278812	−5.62	0.1228	0.3266	−5.17
	PW91PW91/6-31+G**//MP2/6-31+G**			−444.0316058	−7.47	0.1228	0.3266	−7.02

kcal mol⁻¹ at the MP2/6-31+G** level. It is obvious, for a typical cation−π structure, that the binding energy calculated at the MP2 level is very close to that at the PW91PW91, while 2.1 kcal mol⁻¹ more stronger than that at the B3LYP level. We can contribute the difference in binding energy between the MP2 level and the B3LYP level to the influence of dispersion interaction, which will be discussed in the following section. For the distorted cation−π structure obtained at the MP2/6-31+G** level, the BSSE corrected binding energy is also −6.98 kcal mol⁻¹, which is exactly the same as that of the cation−π form.

Electron Correlation. It is well-known that, for the weak interaction system, the influence of electron correlation is important. On the basis of that the optimized structure at the MP2/6-31+G** level, single-point calculations were performed with the HF, B3LYP, and PW91PW91 methods with the basis set of 6-31+G** in order to investigate the effect of electron correlation in the TMA−imidazole and TMA−furan complexes. Since Hartree−Fock theory cannot cover the contribution of electron correlation, the difference in binding energy between the DFT or MP2 method and HF method can be viewed as the contribution of electron correlation (Table 2).

TMA−Imidazole Complex. After the BSSE correction, the binding energies of TMA−imidazole complex are −12.79 kcal mol⁻¹ at the HF level, −15.27 kcal mol⁻¹ at the B3LYP level, −16.86 kcal mol⁻¹ at the PW91PW91 level, and −16.37 kcal mol⁻¹ at the MP2 level. Therefore, for the TMA−imidazole complex, the contributions of electron correlation are 2.5, 4.1, and 3.6 kcal mol⁻¹ for the B3LYP, PW91PW91, and MP2 levels of calculation, respectively. Electron correlation contributes about 20% of total biding energy, which is quite important in the TMA−imidazole system. The electron correlations calculated at the PW91PW91 and the MP2 level are similar. On the other hand, the B3LYP version of DFT method can cover the electron correlation about 1 kcal mol⁻¹ less than that at the PW91PW91 and the MP2 methods. Since the B3LYP approach does not take into account dispersion interaction,[35−37] the

difference in electron correlation between two approaches (1.1 kcal mol⁻¹) can be viewed as, approximately, the contribution of dispersion interactions. This indicates that dispersion interactions contribute ∼7% of total binding energy in the TMA−imidazole system, making a substantial contribution.

TMA−Furan. The contributions of electron correlation in the TMA−furan system predicted by various approaches were also investigated (Table 2). For the typical cation−π form, the BSSE corrected binding energy difference between the B3LYP method and the HF method is about 2.4 kcal mol⁻¹, while the electron correlation estimated at the PW91PW91 and MP2 levels is about 4 kcal mol⁻¹. Considering that, at various theoretical levels, electron correlation enhances about 50% of total binding energy, its influence in TMA−furan system is much more important than that in the TMA−imidzole system. The electron correlation given by the B3LYP approach is about 67% of that by the MP2 approach, and the difference between two methods can be viewed as the dispersion interaction approximately. The dispersion interactions enhance about 19% (1.5 kcal mol⁻¹) in binding energy for the typical cation−π structure.

For the distorted cation−π structure, the electron correlations covered by the B3LYP and MP2 methods are 2.3 and 4.1 kcal mol⁻¹, respectively. Compared with the results of typical cation−π form, the difference in electron correlation between the MP2 and the B3LYP methods increases to 1.8 kcal mol⁻¹. The influence of dispersion interactions in the distorted cation−π form is therefore more important, which is consistent with the geometric characteristics given above. The calculated electron correlation by the PW91PW91 method is always very close to that by the MP2 method. The electron correlation in the PW91PW91 method is 4.1 kcal mol⁻¹, which is exactly the same as the corresponding values at the MP2 level.

Compared with the results of the TMA−imidazole and cation−π form of TMA−furan system at the B3LYP level, the PW91PW91 approach gives smaller TMA−aromatic distances that are similar to the MP2 approach. It seems that the PW91PW91 method is a good choice for investigating the

characteristic of the weak interaction systems. However, the distorted cation−π structure of TMA−furan complex, in which the influence of dispersion interaction is important, cannot be located as the local minimum on the potential energy surface with the PW91PW91 method. The computational result suggests that the PW91PW91 method may not describe the dispersion interaction correctly.

Conclusion

The sliced two-dimensional contour maps of the MEP of furan and imidazole have been used to predicate the possible binding sites in cation−imidazole and cation−furan systems. These predictions are verified by quantum chemistry calculations. For a given cation, similar locations of the negative minima on the MEP maps of aromatic systems may lead to similar cation binding sites in the cation−aromatic systems. Dispersion interactions play an important role since they contributes ∼7% of the total binding energy in the TMA−imidazole system and ∼20% of that in the TMA−furan system. Adding diffuse functions in the basis sets enhances the dispersion interactions in the TMA−aromatic system, thus generating local minimal structures with weaker electrostatic interactions and stronger dispersion interactions. Owning to the influence of the dispersion interactions, using of the MP2 method may yield aberrant optimized structure.

References and Notes

(1) Depriest, S. A.; Mayer, D.; Naylor, C. B.; Marshall, G. R. *J. Am. Chem. Soc.* **1993**, *115*, 5372.
(2) Lin, Z.; Johnson, M. E. *FEBS Lett.* **1995**, *370*, 1.
(3) Kumpf, R. A.; Dougherty, D. A. *Science* **1993**, *261*, 1708.
(4) Ma, J. C.; Dougherty, D. A. *Chem. Rev.* **1997**, *97*, 1303.
(5) Dougherty, D. A. *Science* **1996**, *271*, 163.
(6) Gallivan, J. P.; Dougherty, D. A. *Proc. Natl. Acad. Sci. U.S.A.* **1999**, *96*, 9459.
(7) Kumpf, R. A.; Dougherty, D. A. *Science* **1993**, *261*, 1708.
(8) Zhu, W. L.; Tan, X. J.; Puah, C. M.; Gu, J. D.; Jiang, H. L.; Chen, K. X.; Felder, E., C.; Silman, I.; Sussman, L. J. *J. Phys. Chem. A* **2000**, *104*, 9573.
(9) Tan, X. J.; Jiang, H. L.; Zhu, W. L.; Chen, K., X.; Ji, R., Y. *J. Chem. Soc., Perkin Trans. 2* **1999**, *1*, 107.
(10) Minoux, H.; Chipot, C. *J. Am. Chem. Soc.* **1999**, *121*, 10366.
(11) Sussman, J. L.; Harel, M.; Frolow, F.; Oefner, C.; Goldman, A.; Toker, L.; Silman, I. *Science* **1991**, *25*, 872.
(12) Mecozzi, S.; West, A. P. J.; Dougherty, D. A. *J. Am. Chem. Soc.* **1996**, *118*, 2307.
(13) Kearney, P. C.; Mizoue, L. S.; Kumpf, R. A.; Forman, J. E.; McCrudy, A.; Dougherty, D. A. *J. Am. Chem. Soc.* **1993**, *115*, 9907.
(14) Mecozzi, S.; West, A. P. J.; Dougherty, D. A. *Proc. Natl. Acad. Sci. U.S.A.* **1996**, *93*, 10566.
(15) Pullman, A.; Berthier, G.; Savinelli, R. *J. Am. Chem. Soc.* **1998**, *120*, 8553.
(16) Jiang, H. L.; Zhu, W. L.; Tan, X. J.; Gu, J. D.; Chen, J. Z.; Lin, M. W.; Chen, K. X.; Ji, R. Y. *Sci. China, Ser. B* **1998**, *41*, 535.
(17) Felder, C.; Jiang, H. L.; Zhu, W. L.; Chen, K. X.; Silman, I.; Botti, S.; Sussman, L. J. *J. Phys. Chem. A* **2001**, *105*, 1326.
(18) Szabo, N. G.; Ferenczy, G. G. *Chem. Rev.* **1995**, *95*, 829.
(19) Pepe, G.; Siri, D.; Reboul, P. J. *THEOCHEM* **1992**, *88*, 175.
(20) Gu, J.; Leszczynski, J.; Bansal, M. *Chem. Phys. Lett.* **1999**, *311*, 209.
(21) Pullman, A.; Berthier, G.; Savinelli, R. *J. Comput. Chem.* **1997**, *18*, 2012.
(22) Liu, T.; Gu, J.; Tan, X.-J.; Zhu, W.-L.; Luo, X.-M.; Jiang, H.-L.; Chen, K.-X.; Silman, I.; Sussman, J. L. *J. Phys. Chem. A* **2001**, *105*, 5431.
(23) Zhu, W. L.; Jiang, H. L.; Puah, C. M.; Tan, X. J.; Chen, K. X.; Cao, Y.; Ji, R. Y. *J. Chem. Soc., Perkin Trans. 2* **1999**, *11*, 2615.
(24) Zhu, W. L.; Jiang, H. L.; Tan, X. J.; Chen, J. Z.; Zhai, Y. F.; Gu, J. D.; Lin, M. W.; Chen, K. X.; Ji, R. Y.; Cao, Y. *Acta Chim. Sinica* **1999**, *57*, 852.
(25) Jiang, H. L.; Zhu, W. L.; Tan, X. J.; Chen, J. Z.; Zhai, Y. F.; Liu, D. X.; Zhao, L.; Chen, K. X.; Ji, R. Y. *Acta Chim. Sinica* **1999**, *57*, 860.
(26) Wesolowski, T. A.; Parisel, O.; Ellinger, Y.; Weber, J. *J. Phys. Chem. A* **1997**, *101*, 7818.
(27) Wesolowski, T. A.; Ellinger, Y.; Weber, J. *J. Chem. Phys.* **1998**, *108*, 6078.
(28) Perdew, J. P.; Wang, Y. *Phys. Rev. B* **1992**, *45*, 13244.
(29) Saebo, S.; Almlof, J. *Chem. Phys. Lett.* **1989**, *154*, 83.
(30) Head-Gordon, M.; Head-Gordon, T. *Chem. Phys. Lett.* **1994**, *220*, 122.
(31) Frisch, M. J.; Head-Gordon, M.; Pople, J. A. *Chem. Phys. Lett.* **1990**, *166*, 281.
(32) Head-Gordon, M.; Pople, J. A.; Frisch, M. J. *Chem. Phys. Lett.* **1988**, *153*, 503.
(33) Boys, S. F.; Bernardi, F. *Mol. Phys.* **1970**, *19*, 553.
(34) Frisch, M. J. T., G. W.; Schlegel, H. B.; Scuseria, G. E.; Robb, M. A.; Cheeseman, J. R. Z., V. G.; Montgomery, J. A., Jr.; Stratmann, R. E. B., J. C.; Dapprich, S.; Millam, J. M.; Daniels, A.; D.; Kudin, K. N. S., M. C.; Farkas, O.; Tomasi, J.; Barone, V.; Cossi,; M.; Cammi, R. M., B.; Pomelli, C.; Adamo, C.; Clifford, S.;; Ochterski, J. P., G. A.; Ayala, P. Y.; Cui, Q.; Morokuma, K.; Malick,; D. K.; Rabuck, A. D. R., K.; Foresman, J. B.; Cioslowski, J.;; Ortiz, J. V. B., A. G.; Stefanov, B. B.; Liu, G.; Liashenko, A.; Piskorz,; P.; Komaromi, I. G., R.; Martin, R. L.; Fox, D. J.; Keith, T.; Al-Laham,; M. A.; Peng, C. Y. N., A.; Gonzalez, C.; Challacombe, M.; Gill, P. M. W.; Johnson, B. G.; Chen, W.; Wong, M. W.; Andres, J. L.; Gonzalez, C. H.-G., M.; Replogle, E. S.; Pople, J. A. *Gaussian 98*, Revision A.7; Gaussian, Inc., Pittsburgh, PA, 1998.
(35) Rappe, A. K.; Bernstein, E. R. *J. Phys. Chem. A* **2000**, *104*, 6117.
(36) Kristyan, S.; Pulay, P. *Chem. Phys. Lett.* **1994**, *229*, 175.
(37) Hobza, P.; Sponer, J.; Reschel, T. *J. Comput. Chem.* **1995**, *16*, 1315.
(38) Gu, Y.; Kar, T.; Schenier, S. *J. Am. Chem. Soc.* **1999**, *121*, 9411.
(39) Jeffrey, G. A.; Saenger, W. *Hydrogen Bonding in Biological Structures*; Springer-Verlag: Berlin, 1991.